Charge-transfer process using the molecular-wave-function approach: The asymmetric charge transfer and excitation in Li + Na^+ and Na + Li^+†*

C. F. Melius‡ and W. A. Goddard III
Arthur Amos Noyes Laboratory of Chemical Physics,§ California Institute of Technology, Pasadena, California 91109
(Received 26 September 1973)

The charge-transfer processes occurring in collisions of Li + Na^+ and Na + Li^+ have been studied theoretically using the molecular-wave-function approach. The wave functions and Born-Oppenheimer breakdown terms were evaluated using rigorous methods. The six lowest molecular states (dissociating to the $2s$ and $2p$ atomic states on Li and to the $3s$ and $3p$ atomic states of Na) were included in the coupled equations. The transition probabilities were calculated using linear trajectories for a variety of impact parameters and ion velocities. We find that the over-all transition processes are well represented as a succession of simple two-state transition processes (Σ-Σ, Σ-Π, and Π-Π). The Σ-Σ two-state process can be described in terms of three steps involving (i) a coupling region as the atoms come together [(10–20)a_0], (ii) an uncoupled phase changing region for shorter separatons ($< 10a_0$), and (iii) a decoupling region as the atoms depart [(10–20)a_0]. On the other hand, in the molecular–wave-function formulation, the Σ-Π two-state transition process involves continuous coupling (for $R < 7a_0$). As a result the transition probabilities for Σ-Π coupling differs from that of Σ-Σ coupling, leading to rather different forms for the cross sections.

I. INTRODUCTION

Collisionally induced transitions between electronic states during slow atom-atom collisions are described in the near-adiabatic formalism in which the electronic wave function does not depend on the velocities of the nuclei. Early investigations of the charge-transfer process were carried out by Landau,[1] Zener,[2] and Stueckelberg.[3] They obtained an estimate of the two-state transition probability for two potential-energy curves having a crossing or a near crossing (giving rise to the Landau-Zener-Stueckelberg approximation).[4] Estimates of the charge-transfer probability between two near-resonant electronic states have been considered by Gurnee and Magee,[5] Rapp and Francis,[6] and others.[7-11]

These approaches usually take the electronic states to be atomic eigenstates. On the other hand, one can take the electronic states to be molecular wave functions obtained from the Born-Oppenheimer (BO) approximation.[12] Within the BO approximation the electron readjusts adiabatically to the instantaneous positions of the nuclei. Thus, in order to describe collisionally induced processes such as electronic excitation, electron transfer, or electronic excitation transfer, it is necessary to include terms neglected in the BO approximation (called the BO breakdown or BO coupling terms). This molecular–wave-function approach has been applied to several charge-transfer systems.[13-19] In particular the rotational coupling to Π states has recently been considered.[13-15] However, difficulties exist in this procedure, both in the evaluation of the molecular wave functions and energy curves and in the evaluation of the coupling terms between the molecular states.[20]

Herein, we report the use of the multistate molecular–wave-function approach to obtain electronic transition cross sections for the collisions

$$\mathrm{Li} + \mathrm{Na}^+ \rightarrow \mathrm{Li}^+ + \mathrm{Na} \tag{1}$$

and

$$\mathrm{Na} + \mathrm{Li}^+ \rightarrow \mathrm{Na}^+ + \mathrm{Li}. \tag{2}$$

Both the molecular wave functions and coupling terms are evaluated rigorously, including Π states as well as Σ states. The results of the full (six-state) calculations are analyzed in terms of elementary transition processes. We find that the results can be interpreted in terms of a simple picture involving a succession of several two-state transitions, each of which involves characteristic internuclear separations depending upon the nature of the states.

II. DETAILS OF THE METHOD

A. Coupled equations

The total wave function Ψ for the scattering system can be expressed in the time-independent representation as a function of the internuclear coordinate ($\vec{R}$) and the electronic coordinates (taken collectively as $\vec{r}$). Since the nuclear masses are much greater than the electronic mass, it is convenient to expand the total wave function as

$$\Psi = \sum_i F_i(\vec{R})\psi_i(\vec{r}, R), \tag{3}$$

where ψ_i describes a given electronic state of the system (which may depend on the internuclear separation but not on the orientation of the molecule in space) and F_i describes the nuclear motion for the given electronic state ψ_i.

Substituting Eq. (3) into the time-independent Schrödinger equation, multiplying on the left by ψ_j, and integrating over the electronic coordinates, leads to the set of coupled equations for the nuclear motion[21]:

$$\sum_i \left[S_{ij}\left(-\frac{1}{2M}\nabla_R^2 - E\right) + V_{ij}(R) + \frac{J_{ji}}{M} - \frac{\vec{\Gamma}_{ji}}{M}\cdot\vec{\nabla}_R \right] F_i(\vec{R}) = 0, \quad (4)$$

where

$$S_{ij} = \langle \psi_i | \psi_j \rangle, \quad (5a)$$

$$V_{ij} = S_{ij}(Z_A Z_B/R) + \langle \psi_i | \mathcal{H}_{el} | \psi_j \rangle, \quad (5b)$$

$$\vec{\Gamma}_{ij} = \langle \psi_i | \vec{\nabla}_R | \psi_j \rangle, \quad (5c)$$

$$J_{ij} = \langle \psi_i | -\tfrac{1}{2}\nabla_R^2 | \psi_j \rangle, \quad (5d)$$

and $\mathcal{H}_{el}$ is the electronic Hamiltonian.

While Eq. (4) is exact, it involves an infinite number of states (including the continuum). To be computationally feasible, it is necessary to choose a representation for ψ_i so that Eq. (3) can be approximated in terms of a small number of states. One approach is to take ψ_i to be the atomic eigenfunctions of the separated atoms. This is a good approximation for sufficiently large nuclear velocities such that the nuclei move as fast as the valence electrons (e.g., for Li, the velocity of the valence electron is ~10^8 cm/sec, which corresponds for $LiNa^+$ to a Na^+ ion energy of ~120 keV). For slow nuclear velocities (i.e., $v < 10^8$ cm/sec), the electron is best described in terms of molecular wave functions ψ_i defined as the eigenfunctions of the electronic Hamiltonian,

$$\mathcal{H}_{el}\psi_i(\vec{r}, R) = E_i(R)\psi_i(\vec{r}, R). \quad (6)$$

In this case the electronic wave functions are orthogonal,

$$S_{ij} = \delta_{ij},$$

and the potential matrix is diagonal,

$$V_{ij} = \delta_{ij}V_i(R).$$

The $V_i(R)$ are called the potential-energy curves (surfaces). Each $V_i(R)$ represents the BO potential curve (surface) on which the nuclei move, given that the electrons are in the eigenstate ψ_i. In general, the nuclear motion $F_i(\vec{R})$ for the various electronic states ψ_i are coupled through the terms $\vec{\Gamma}_{ij}$ and J_{ij} [Eq. (4)]. However, as we will show below, for slow nuclear velocities, the coupling between F_i's will be small except where the potential-energy differences are small. Thus, for small velocities the use of (6) should be appropriate.

In this paper we will be primarily concerned with ion energies that are large compared to the change in electronic energy with R,

$$E \gg V_i(R) - V_i(\infty);$$

that is, $E > 100$ eV. For such energies, we can assume that the trajectory of the ion is essentially a straight line.[22] With this approximation (called the impact-parameter approach),[23] the nuclear wave function can be written as

$$F_i(\vec{R}) = a_i(z)\exp\left(i\int_{-\infty}^{z} k_i(z')\,dz'\right), \quad (7)$$

where $z^2 + b^2 = R^2$, b is the impact parameter, R is the internuclear distance (z, b, and R are defined in Fig. 1), $k_i = [2M(E - V_i)]^{1/2}$ is the momentum of the moving atom (the other atom is taken as stationary), and V_i is the potential energy of the ith molecular state. Substituting Eq. (7) into Eq. (4), taking $k_i = k_j \approx k = Mv$, and ignoring terms of order $1/M$ compared to $1/m_e$, we obtain

$$\frac{da_i(z)}{dz} = -\sum_j \Gamma_{ij}(z)\,e^{-i\omega_{ij}(z)}a_j(z), \quad (8)$$

where

$$\omega_{ij}(z) = \frac{1}{v}\int_{-\infty}^{z}(V_j - V_i)\,dz' \quad (9)$$

and

$$\Gamma_{ij}(z) = \langle \psi_i | \frac{\partial}{\partial z} | \psi_j \rangle. \quad (10)$$

Given the initial conditions, $\{a_i(-\infty)\}$, the coupled equations (8) are solved to obtain the $\{a_i(z)\}$.[24] Substituting these into (7) and in turn into (3) then determines the total wave function of the system.

The Γ_{ij}'s represent the nonadiabatic coupling terms between molecular states due to the breakdown of the Born-Oppenheimer approximation. It is convenient to divide Γ_{ij} into its radial and angu-

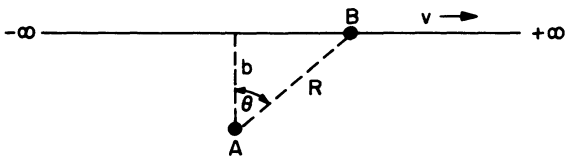

FIG. 1. Collision geometry. The projectile (B) moves with a constant velocity along the z axis from $z = -\infty$ to $z = +\infty$, passing the target (A) at an impact parameter b. Thus, the internuclear distance R is related to b and z by $R^2 = z^2 + b^2$.

lar parts,

$$\Gamma_{ij} = (z/R) M_{ij} + (b/R) N_{ij}, \tag{11}$$

where

$$M_{ij} = \langle \psi_i | \frac{\partial}{\partial R} | \psi_i \rangle, \tag{12a}$$

$$N_{ij} = \langle \psi_i | \frac{1}{R} \frac{\partial}{\partial \theta} | \psi_j \rangle. \tag{12b}$$

The radial term M_{ij} couples states of the same symmetry (e.g., Σ-Σ, Π-Π, etc.), while the angular term N_{ij} couples states with angular momentum differing by one (e.g., Σ-Π).

B. Molecular eigenstates

In order to obtain the molecular wave functions ψ_i, we must solve (6). This is a thirteen-electron problem for $LiNa^+$; however, twelve of these electrons are in orbitals (the core orbitals of Li^+ and Na^+) that remain essentially unchanged over the range of R of interest here. Thus, the $LiNa^+$ quasimolecule involves only one electron whose state changes with R and can be treated as a one-electron system, if we can find some effective potential to represent the Li^+ and Na^+ cores.

There have been many efforts toward developing such pseudopotentials using empirical potentials that are adjusted to reproduce some of the atomic energies.[25] However, we wish to calculate not only the electronic energies, but also the coupling terms M_{ij} and N_{ij} which could depend sensitively upon the shapes of the wave functions. We have therefore used an effective potential method which is based on reproducing both the energies *and* wave functions. This method is described in detail elsewhere[26] and it should suffice to indicate some of its features and limitations:

(i) The effective potential is based on *ab initio* Hartree-Fock (HF) orbitals for the ground and excited states of the atoms and is constructed so that its eigenfunctions are smooth in the core region (i.e., HF orbitals without core character). The resulting effective potentials (called coreless HF effective potentials or CHF EP) contain repulsive terms that simulate the effect of the Pauli principle (which is usually incorporated by using valence orbitals orthogonal to the core).

(ii) The resulting CHF EP's are simple functions of r (no operators) but *must* be allowed to be different for s states, p states, etc. That is, the CHF EP's are angular-momentum dependent. General programs were developed to evaluate (analytically) the multicenter molecular integrals resulting from the use of such angular-momentum dependent potentials. (These programs are sufficiently fast that the computation time to solve for the various electronic states at a given R is governed by the time to diagonalize the resulting one-electron Hamiltonian matrix.)

(iii) For the Σ states, the basis set used to expand the valence orbitals consisted of three sets of s functions, three sets of p functions, and one set of d functions, appropriate for describing the lowest ^2S and ^2P states of each atom. For the Π states, the basis set was modified by deleting the s functions and adding a second set of d functions to each center.

(iv) In evaluating the potential energy curves, we have *not* included the repulsive effects due to the interaction between the Li^+ and the Na^+ ion cores. This repulsive term is not important for our calculations since the coupled equations (8) depend only on the differences between the potential energy curves.

(v) The effective potential method breaks down for small R ($<3.5a_0$), since it assumes that the core orbitals do not change with R. (This is not valid when the cores begin to overlap.) However, the dominant charge-transfer processes occur at long range (see Sec. IV), so that a detailed knowledge of the potential-energy curves and coupling terms at small R ($<3.5a_0$) is not necessary. We found that modification of the potential energy curves and coupling terms for $R < 3.5a_0$ did not change the total charge-transfer cross sections significantly. [For differential scattering cross sections at large angle, on the other hand, serious errors could result. This also holds for (iv)].

(vi) The HF description of the alkali-metal atoms leads to a small error in the ionization energies for the various atomic states. Although not large even small errors in the relative energies of electronic states on different atoms can lead to significant effects upon the charge-transfer cross sections. For example, the difference between the ionization energies (i.e., the energy defect) of Li($2s$) and Na($3s$) should be 0.0093 Hartree = 0.25 eV rather than 0.0141 Hartree = 0.038 eV. To alleviate this difficulty (which arises from many-body effects involving the core electrons), the resulting potential energy curves of $LiNa^+$ have been shifted slightly to reproduce the experimental ionization energies of the atoms.

C. Evaluation of the coupling matrix elements

The coupling terms M_{ij} and N_{ij} are evaluated by substituting the molecular wave functions from (6) into Eqs. (12). As a simplifying approximation, we take the masses of the nuclei to be infinitely heavy. This is consistent with the impact parameter approximation, which ignores terms of order m/M. However, the resulting values for M_{ij} and

N_{ij} are not unique in that they depend upon the particular reference frame chosen for the coordinate system.[27] This is illustrated in Fig. 2, which shows the coupling term M_{12} between the $1\,^2\Sigma^+$ and $2\,^2\Sigma^+$ states of $LiNa^+$ as obtained using different reference frames.

While the coupling terms Γ_{ij} differ for various reference frames, the solution of Eq. (8) will yield an equivalent result for any given set of Γ_{ij} providing (i) the proper boundary conditions are defined, and (ii) the complete electronic space (including the continuum states of ψ_i) is used in the coupled equations of (8). Serious errors may result, however, if the coupled equations are restricted to a small number of states. (The errors result from attempting to describe an orbital moving through space in terms of a finite number of functions located in a fixed reference frame.)

In order to obtain meaningful solutions to Eq. (8) using a finite number of coupled equations, one must account for the translational motion of the electron. The usual method has been to introduce traveling phase factors into the molecular orbitals.[27-30] However, this method involves evaluation of complex integrals which cannot in the low-velocity region be simplified through expansion in a power series in velocity. We will present an alternative method for determining Γ_{ij} in the low-velocity region. First, however, it is appropriate to discuss the limitations of the traveling phase factor method.

1. *Traveling phase factors*

Introduction of traveling phase factors leads to a molecular wave function of the form

$$\psi_j^{\mathrm{TO}} = \psi_j \exp(-ip_j \vec{v}\cdot\vec{r}) \exp\left[-i\,\frac{1}{v}\int^z \left(\epsilon_j + p_j^2\,\frac{v^2}{2}\right) dz\right], \tag{13}$$

satisfying the incoming and outgoing boundary conditions for Eq. (8). However, while introduction of phase factors is straightforward for the atomic eigenfunction representation[31] (where each atomic basis function follows the position of a specific atomic nucleus), the use of phase factors in molecular wave functions is somewhat arbitrary, depending upon the choice of $p_j(\vec{r}, R)$ in (13). While the various definitions of ψ^{TO} would be equivalent at $R=\infty$, the resulting coupling terms between states can be quite different for finite R.

As an example, consider the $1\,^2\Sigma^+$-$2\,^2\Sigma^+$ coupling terms of $LiNa^+$ as evaluated using various definitions of ψ^{TO} in the limit that $v \to 0$. (For the traveling orbital wave function, the coupling operator Γ must include the electronic Hamiltonian, i.e.,

$$\Gamma_{ij}^{\mathrm{TO}} = \langle \psi_i^{\mathrm{TO}} | \left(\frac{\partial}{\partial z} - \frac{\mathcal{H}_{\mathrm{el}}}{iv}\right) | \psi_j^{\mathrm{TO}} \rangle \tag{14}$$

since the ψ^{TO}'s are not longer eigenfunctions of $\mathcal{H}_{\mathrm{el}}$.) For the Bates and McCarroll[27] definition of the traveling orbital (denoted ψ_i^{BM}), we have ($z=R$)

$$M_{12}^{\mathrm{BM}} = \langle (1\,^2\Sigma^+)^{\mathrm{BM}} | \left(\frac{\partial}{\partial z} - \frac{\mathcal{H}_{\mathrm{el}}}{iv}\right) | (2\,^2\Sigma^+)^{\mathrm{BM}} \rangle$$

$$= \langle 1\,^2\Sigma^+ | \frac{\partial}{\partial z} | 2\,^2\Sigma^+ \rangle_{\mathrm{Na}}, \tag{15}$$

while

$$M_{21}^{\mathrm{BM}} = \langle (2\,^2\Sigma^+)^{\mathrm{BM}} | \left(\frac{\partial}{\partial z} - \frac{\mathcal{H}_{\mathrm{el}}}{iv}\right) | (1\,^2\Sigma^+)^{\mathrm{BM}} \rangle$$

$$= -\langle 1\,^2\Sigma^+ | \frac{\partial}{\partial z} | 2\,^2\Sigma^+ \rangle_{\mathrm{Li}}, \tag{16}$$

which are shown in Fig. 2 (depicted by long dashed lines). One could define a generalized traveling orbital by attaching a separate phase factor to each of the atomic centered basis functions used to express ψ_i. Using the generalized traveling orbital definition, one would obtain the pair of coupling terms M_{12}^{GTO} and M_{21}^{GTO}, which are also shown in Fig. 2 (depicted by short dashed lines).

As one can see from Fig. 2, the different definitions of the traveling orbitals lead to quite different coupling terms. Furthermore, choosing other functional forms for p_j in Eq. (13) would lead to still different values for the coupling terms. Even the values of M_{12}^{GTO} and M_{21}^{GTO} would not be unique since they depend upon the basis set used to express ψ_i.

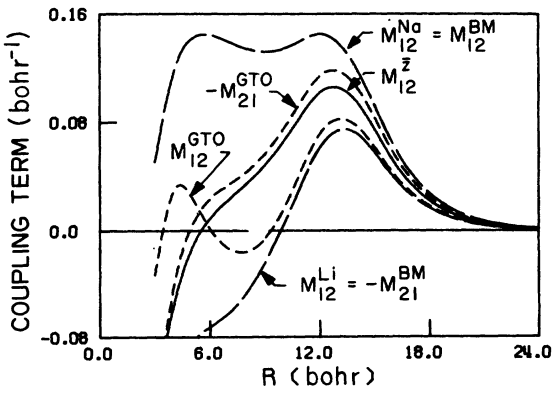

FIG. 2. The coupling term $M_{12} = \langle \psi_1 | \partial/\partial R | \psi_2 \rangle$ between the $1\,^2\Sigma^+$ and $2\,^2\Sigma^+$ states of $LiNa^+$. M_{12}^{Li}, M_{12}^{Na}, and $M_{12}^{\bar{z}}$ correspond to the origin being located at the Li atom, the Na atom, and $\bar{z}$, respectively. BM and GTO indicate the Bates-McCarrol and the generalized-traveling-orbital definitions. M_{12}^{BM} and M_{21}^{BM} [defined by Eq. (14) and (15)] correspond to M_{12}^{Na} and $-M_{12}^{\mathrm{Li}}$, respectively. Note that $M_{12}^{\mathrm{BM}} \neq -M_{12}^{\mathrm{BM}}$ and $M_{12}^{\mathrm{GTO}} \neq -M_{21}^{\mathrm{GTO}}$, owing to the essential singularity in the phase factors.

The phase factors are necessary for high velocities in order to properly represent the translational momentum of the electron. However, in the low-energy regime (for which the molecular-wave-function approach is appropriate), the translational momentum of the electron is small compared to its instantaneous momentum. Thus, one would hope to simplify the computational effort introduced by the traveling phase factors by, for example, expanding in a power series in velocity and keeping only the lowest order terms. Unfortunately, this is not possible for the phase factors in Eq. (13).

In the limit that $v \to 0$, each of the various definitions of ψ_i^{TO} differ from ψ_i only by a multiplicative phase constant. However, this phase constant is undefined when $v = 0$. This leads to an inconsistency in the traveling orbital method when $v = 0$, since we then have

$$S_{12}^{\mathrm{TO}}(R) = \langle \psi_1^{\mathrm{TO}}(\vec{r}, R) | \psi_2^{\mathrm{TO}}(\vec{r}, R) \rangle = 0, \tag{17}$$

while

$$\frac{d}{dR} S_{12}^{\mathrm{TO}}(R) \neq 0. \tag{18}$$

Thus the coupling operator is not anti-Hermitian even when the velocity is zero, leading to $M_{ij}^{\mathrm{TO}} \neq -M_{ji}^{\mathrm{TO}}$ (see Fig. 2). Attempts to simplify the coupled equations by taking the low-velocity limit as $S_{ij} = \delta_{ij}$ can, therefore, destroy probability conservation and detailed balancing.[32] (The difficulty in the zero-velocity approximation of the traveling orbital method occurs because the ψ_i^{TO}'s contain an essential singularity in v at $v = 0$. Thus, the coupled equations cannot be expanded in a power series in velocity for small velocity.)

2. *"Center of electron" coordinate system*

Since we are interested in collisions occurring in the low-energy regime[33] for which the translational momentum of the electron is not overly important, we have formulated an alternative, simple approximation for the evaluation of Γ_{ij} without the need of phase factors.[34]

We define the reference frame for evaluating the coupling term to be that of the electron. Since the electron's position is described by a wave function, the coupling matrix element is defined as an average of the resultant coupling terms evaluated for various origins but weighted by a term related to the probability of the electron being at that point in space both before and after the transition, i.e.,

$$\bar{\Gamma}_{ij} = \int d^3r \, \rho_{ij}(\vec{r}) \Gamma_{ij}(\vec{r}) \Big/ \int d^3r \, \rho_{ij}(\vec{r}), \tag{19}$$

where $\Gamma_{ij}(\vec{r})$ is the coupling term evaluated using $\vec{r}$ as the origin and $\rho_{ij}(\vec{r})$ is the weighting function for that point $\vec{r}$. In (19) we chose $\rho_{ij}(\vec{r})$ to be[35]

$$\rho_{ij}(\vec{r}) = |\psi_i(\vec{r}) \psi_j(\vec{r})|. \tag{20}$$

For diatomic molecules, $\Gamma_{ij}(\vec{r})$ is a linear function of the distance z along the internuclear axis (not to be confused with z of the impact parameter method), and hence one can find a point $\vec{\bar{r}} = \bar{z}$ ($\bar{x} = 0$, $\bar{y} = 0$), such that

$$\int d^3r \, \rho_{ij}(\vec{r})(z - \bar{z}) = 0. \tag{21}$$

The $\bar{\Gamma}_{ij}$ of Eq. (19) can therefore be replaced by

$$\bar{\Gamma}_{ij} = \Gamma_{ij}^{\bar{z}}, \tag{22}$$

where $\bar{z}$ specifies the origin of the coordinate system in which Γ_{ij} is evaluated. The resulting coupling term $M_{12}^{\bar{z}} = \langle 1 | \partial / \partial R | 2 \rangle_{\bar{z}}$ is shown for $LiNa^+$ in Fig. 2.

In actually evaluating Γ_{ij}, the R and θ dependence of $\psi_i(\vec{r}, R)$ as a function of R must be known. Each electronic state ψ_i is calculated in terms of a basis-set expansion

$$\psi_i(\vec{r}, R) = \sum_\mu \chi_\mu(\vec{r}, R) C_{\mu i}(R), \tag{23}$$

which defines $C_{\mu i}(R)$ for a grid of points in R. Since $C_{\mu i}$ does not depend upon θ, N_{ij} may be evaluated directly using the known analytic form of $\partial \chi_\mu / \partial \theta$. On the other hand, M_{ij} requires both $\partial C_{\mu i} / \partial R$ as well as $\partial \chi_\mu / \partial R$, but $C_{\mu i}(R)$ is only known at a discrete number of points. We have therefore evaluated M_{ij} as

$$\begin{aligned} M_{ij} &= \langle \psi_i | \frac{\partial}{\partial R} | \psi_j \rangle \\ &= \lim_{\lambda \to 0} \frac{1}{\lambda} [\langle \psi_i(R) | \psi_j(R + \lambda) \rangle - \langle \psi_i(R) | \psi_j(R) \rangle] \\ &= \lim_{\lambda \to 0} \frac{1}{\lambda} \langle \psi_i(R) | \psi_j(R + \lambda) \rangle - \delta_{ij} \end{aligned} \tag{24}$$

[since $\langle \psi_i(R) | \psi_j(R) \rangle = \delta_{ij}$]. We found that a value of $\lambda = 0.001 a_0$ provides reliable results (negligible second-order terms).

III. RESULTS

The methods described in the previous section were applied to the collisions[36]

$$\mathrm{Li} + \mathrm{Na}^+ \tag{25}$$

and

$$\mathrm{Na} + \mathrm{Li}^+, \tag{26}$$

using the six lowest molecular states of $LiNa^+$. These states (four Σ states and two Π states) represent all the states dissociating either to the

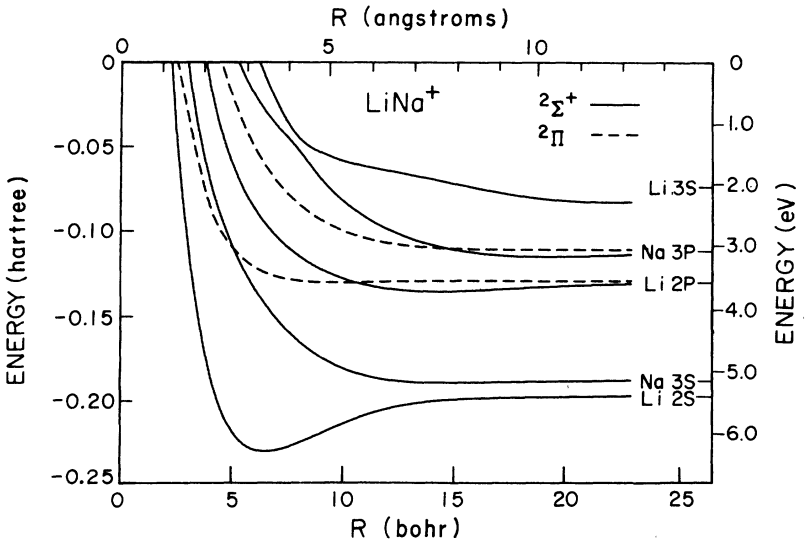

FIG. 3. The potential-energy curves for the $LiNa^+$ molecule. Solid curves, $^2\Sigma^+$ states; dashed curves, $^2\Pi$ states. [Atomic units ($\hbar = e = m_e = 1$) are used: 1 Hartree = 27.2117 eV, 1 bohr = 0.52917 Å].

$2\,^2S$ or $2\,^2P$ states of Li or to the $3\,^2S$ or $3\,^2P$ states of Na. The calculated potential energy curves for these states are shown in Fig. 3. The radial coupling terms M_{ij} [Eq. (12a)] are shown in Fig. 4(a), while the angular coupling terms N_{ij} [Eq. (12b)] are shown in Fig. 4(b) (but with the $1/R$ factor removed, i.e., $\langle \Sigma | \partial/\partial\theta | \Pi \rangle = RN_{ij}$ is plotted).

The resulting total charge transfer cross sections for $Li + Na^+$ and $Na + Li^+$ are shown in Fig. 5 and compared with the experimental results of Daley and Perel.[37] We see that the theoretical and experimental results are in very good agreement, not only for the magnitudes of the absolute cross sections, but also for the amplitudes and phases of the oscillatory structure. Furthermore, the theoretical results lead correctly to a slightly smaller charge transfer cross section for $Li + Na^+$ than for $Na + Li^+$. (The estimated uncertainty in the absolute magnitude for either experimental cross

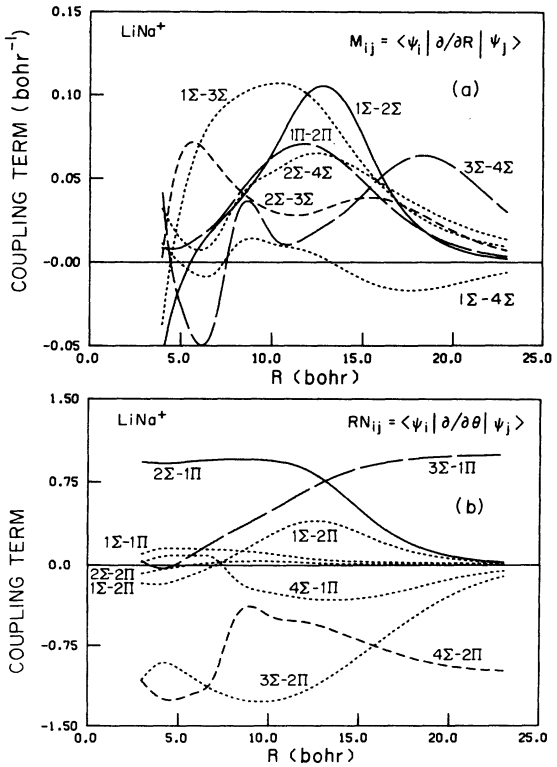

FIG. 4. (a) The radial coupling terms $M_{ij} = \langle \psi_i | \partial/\partial R | \psi_j \rangle$ between the various molecular states of $LiNa^+$; (b) The angular coupling terms $RN_{ij} = \langle \Psi_i | \partial/\partial\theta | \Psi_j \rangle$ between the various molecular states of $LiNa^+$.

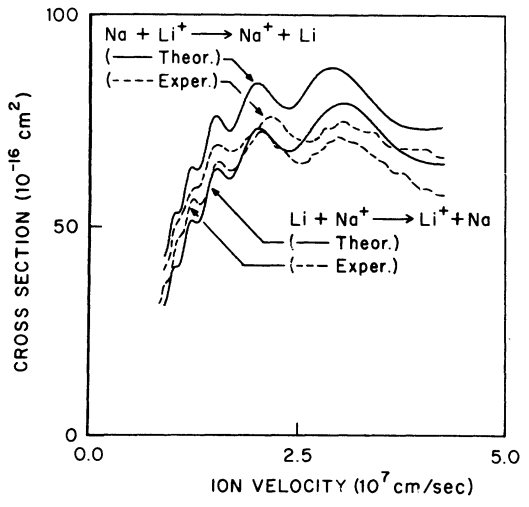

FIG. 5. Comparison of the theoretical (six-state) and experimental cross sections for $Li + Na^+ \rightarrow Li^+ + Na$ and $Na + Li^+ \rightarrow Na^+ + Li$. Estimated error in the absolute values of the experimental total cross sections is 10%.

sections is 10%.[38]) Inclusion of the six molecular states should adequately represent the total charge-transfer process for these cases (with the electron starting in the lowest state of one of the atoms). Hence the main error in the theoretical cross sections is probably due to the neglect of translational momentum of the electrons. Inclusion of electron translational momentum will lead to a decrease in the charge-transfer transition probabilities (since the electron must change direction), and the error in the theoretical cross sections should increase with ion velocity.[39]

IV. DISCUSSION

In the previous section, we found that the molecular-wave-function approach can provide an accurate description of charge-transfer cross sections (including the detailed structure) and can distinguish properly between such similar collisions as $Li+Na^+$ and $Na+Li^+$. However, the motivation in carrying out such theoretical calculations is *not* just to obtain accurate numbers. Rather, we also want to understand the detailed mechanisms involved in the processes so that we can learn how the final cross sections are determined by various aspects of the molecular wave functions and potential energy curves. In this way we would hope to build sufficient understanding of the processes that qualitative predictions could be made for other systems without carrying out detailed coupled-state calculations. With this motivation, we will now analyze the charge-transfer results.

A. Cross sections for transitions to individual states

For $LiNa^+$, the energy defect $|\Delta E|$ between the ground states for the two atoms [Li(2s) and Na(3s)] is 0.0093 Hartree (0.25 eV), while the next higher state [Li(2p)] is 0.0586 Hartree(1.59 eV) above the Na(3s) state. Thus, we have a near-resonance between the Li(2s) and Na(3s) states. As a result, the two-state approximation (involving coupling only between the $1\,^2\Sigma^+$ and $2\,^2\Sigma^+$ states) should yield a reasonable estimate of the charge-transfer cross section.

In order to determine the relative importance of the $1\,^2\Sigma^+ \rightarrow 2\,^2\Sigma^+$ transition as compared to the other transitions that could occur, we carried out three sets of calculations:

(i) two states ($1\,^2\Sigma^+$, $2\,^2\Sigma^+$),

(ii) three states ($1\,^2\Sigma^+$, $2\,^2\Sigma^+$, $1\,^2\Pi$),

(iii) six states ($1\,^2\Sigma^+$, $2\,^2\Sigma^+$, $3\,^2\Sigma^+$, $4\,^2\Sigma^+$, $1\,^2\Pi$, $2\,^2\Pi$)

for both (1) and (2). The resulting cross sections are given in Fig. 6, where we see that as expected, the cross sections are dominated by transitions between the two lowest $^2\Sigma^+$ states. The transition to the Li $2p\pi$ state is also somewhat important, particularly for the process $Na+Li^+$, where the $Na(3s) \rightarrow Li(2p\pi)$ transition dominates the $Na(3s) \rightarrow Li(2s)$ transition for low energies (i.e., $v \lesssim 7 \times 10^6$ cm/sec or Li^+ ion energies $\lesssim$170 eV). Cross sections to other states are considerably smaller.

We see that the oscillations in the total cross section are found in the two-state, three-state, and six-state calculations, and hence are due to the $1\,^2\Sigma^+ \rightarrow 2\,^2\Sigma^+$ transition. However, although the oscillations have approximately the same frequency and amplitude in the various calculations, the *phase* of the oscillations in the two-state calculations is different from that obtained in the three- and six-state calculations (both of which include the $1\,^2\Pi$ state). Thus the differences in the total cross sections for processes (1) and (2) (Fig. 5)

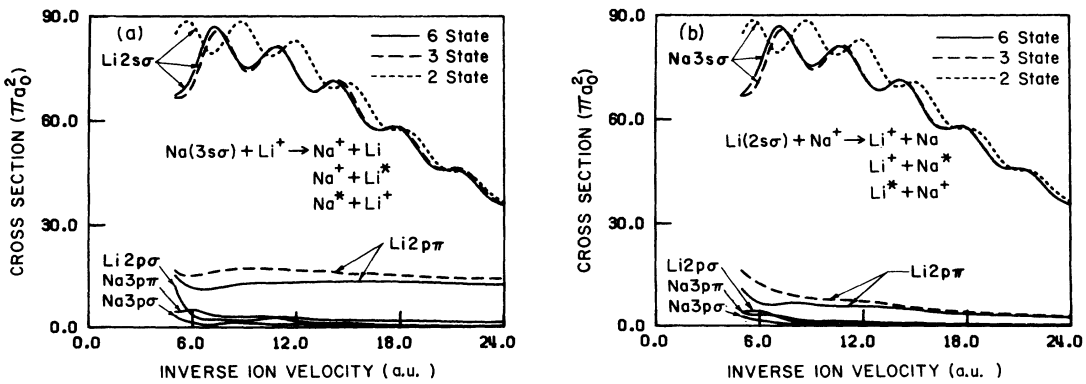

FIG. 6. Comparison of the theoretical cross sections to individual atomic states using six-state (solid), three-state (dashed), and two-state (dotted) approximations for collisions of $Na + Li^+$ and $Li + Na^+$ (1 a.u. velocity $= 2.18 \times 10^8$ cm/sec; $\pi a_0^2 = 0.879 \times 10^{-16}$ cm^2).

result essentially from added contributions involving the $1\,^2\Pi$ state (not included in the two-state approximation).

From Fig. 6 we see that the three- and six-state calculations lead to essentially identical cross sections for the $1\,^2\Sigma^+ \rightarrow 2\,^2\Sigma^+$ transition, both in amplitude and oscillatory structure. On the other hand, the cross section for the transition to the $1\,^2\Pi$ state in the three-state approximation corresponds to the sum of the cross sections for transitions into the $1\,^2\Pi$, $2\,^2\Pi$, $3\,^2\Sigma^+$, and $4\,^2\Sigma^+$ states in the six-state approximation. Thus, the three-state approximation leads to a fair description of the collision processes in (1) and (2). [For high velocities ($v > 0.2$ a.u. $= 4\times10^7$ cm/sec), the three-state approximation breaks down as transitions to the higher lying states become important.]

We will now analyze the various coupling processes in order to learn the origins of the various results presented above. First, we will examine the two different types of two-state coupling processes that occur in the molecular-wave-function approach: (i) radially induced transitions between states of the same symmetry (e.g., Σ-Σ and Π-Π) and (ii) rotationally induced transitions between states of different symmetries (e.g., Σ-Π).

B. Two-state Σ-Σ coupling process

The simplest two-state process involves symmetric, resonant charge transfer[5,6,40] as in

$$\mathrm{Na}(3s) + \mathrm{Na}^+ \rightarrow \mathrm{Na}^+ + \mathrm{Na}(3s). \tag{27}$$

For the symmetric case, the two relevant molecular states are of different symmetries (Σ_g and Σ_u). Therefore, there is no coupling between the two states ($M_{gu} = 0$). However, the initial-state wave function at $z = -\infty$ is a linear combination of the two molecular states, i.e.,

$$\Psi(z = -\infty) = 2^{-1/2}(\psi_g + e^{i\phi(z=-\infty)}\psi_u),$$

where ϕ is the relative phase between the two states. Since each molecular state corresponds to motion on a different potential energy curve, the evolution of the phase factor for each state [see Eq. (7)] is different. Thus, even though $M_{gu} = 0$, ϕ does not remain constant.

The resulting transition probability is given by

$$P(v, b) = \sin^2(\tfrac{1}{2}\Delta\phi), \tag{28}$$

where $\Delta\phi$ is the change in the relative phase between the states, i.e.,

$$\Delta\phi = \frac{1}{v}\int_{-\infty}^{\infty}(V_g - V_u)\,dz \tag{29a}$$

$$= \frac{2}{v}\int_b^{\infty}\frac{R[V_g(R) - V_u(R)]}{(R^2 - b^2)^{1/2}}\,dR. \tag{29b}$$

We see from (28) that the charge transfer probability P is maximum when the relative phase changes differ by π ($\Delta\phi = \pi, 3\pi, \ldots$), while the charge transfer probability is zero if the two states are in phase (i.e., $\Delta\phi = 0, 2\pi, \ldots$). Furthermore, we see from (29) that for a given b and v the charge transfer probability depends only upon a path integral of the energy difference $(V_g - V_u)$.

As an example, in Fig. 7, we show the energy difference between the $1\,^2\Sigma_g^+$ and $1\,^2\Sigma_u^+$ states for Na_2^+. The resulting $P(v, b)$ for process (27) is shown in Fig. 8(a) as a function of b for various v. As the impact parameter decreases, the energy difference at $R = b$ increases and P oscillates rather

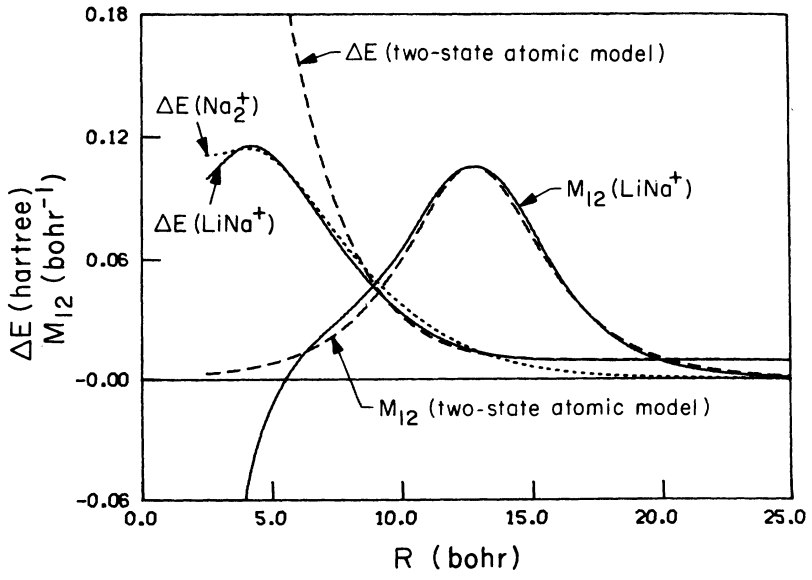

FIG. 7. The potential energy difference curves [$\Delta E = V_2(R) - V_1(R)$] for Na_2^+ (dotted line), $LiNa^+$ (solid line), and the two-state atomic model (dashed line) for $LiNa^+$. Also plotted are the coupling terms M_{12} for $LiNa^+$ (solid line) and the two-state atomic model (dashed line) for $LiNa^+$.

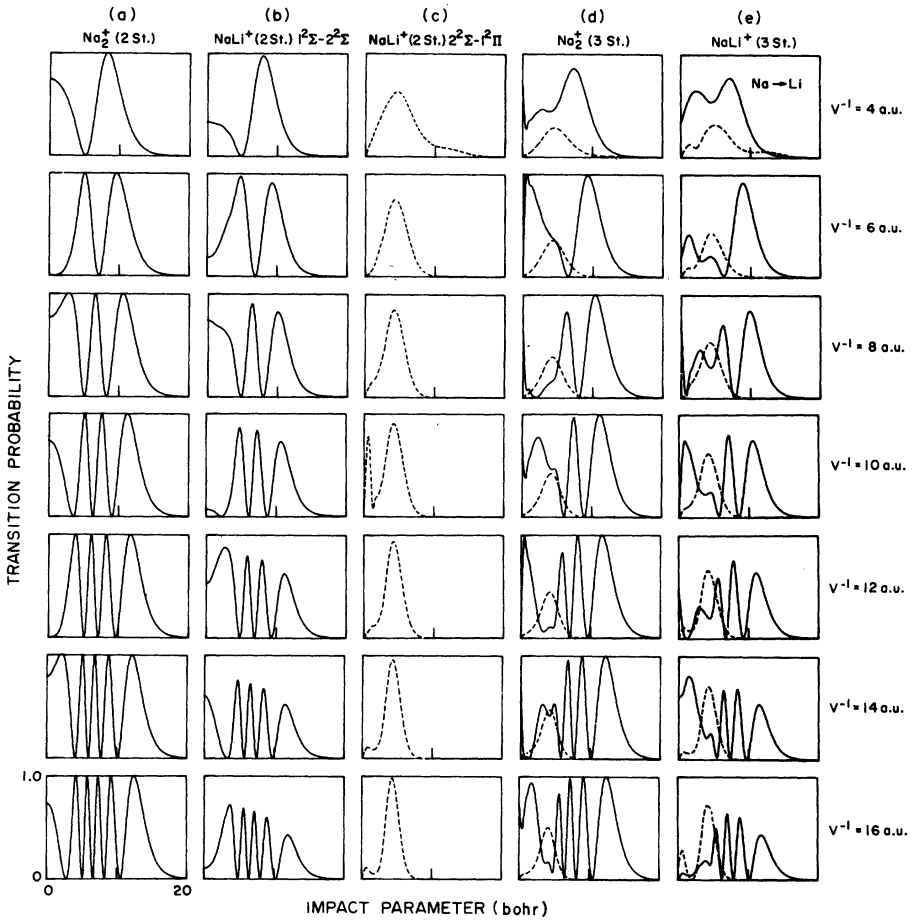

FIG. 8. The transition probabilities $P(v,b)$ as a function of impact parameter b for various velocities for (a) $Na + Na^+$ ($1\,^2\Sigma_g^+$, $1\,^2\Sigma_u^+$ two-state); (b) $Na + Li^+$ ($1\,^2\Sigma^+$, $2\,^2\Sigma^+$, two-state); (c) $Na + Li^+$ ($2\,^2\Sigma^+$, $1\,^2\Pi$ two-state); (d) $Na + Na^+$ ($1\,^2\Sigma_g^+$, $1\,^2\Sigma_u^+$, $1\,^2\Pi_u$ three-state); and (e) $Na + Li^+$ ($1\,^2\Sigma^+$, $2\,^2\Sigma^+$, $1\,^2\Pi$ three-state). Solid lines indicate Σ-Σ coupling; dotted lines indicate Σ-Π coupling.

uniformly. However, due to a maximum in the energy difference $[R_{max}(Na_2^+) \approx 4.0a_0]$, the rate of oscillation is decreased for impact parameters smaller than R_{max}, leading to oscillations in the total cross section.[41,42] The total cross section σ for process (27) in the two-state approximation is shown in Fig. 9. As expected from (29) the spacing in the oscillations in σ is proportional to v^{-1}.

We now consider the near-resonant two-state charge transfer process in $LiNa^+$. In this case, the coupling term between the two states ($M_{12} = \langle \psi_1 | \partial/\partial R | \psi_2 \rangle$) is not zero. The coupling term $M_{12}(R)$ represents essentially the process of molecular formation, that is, the atomic orbitals at large R ($>20a_0$),

$$\psi_1 = \phi_{Li(2s)}\,, \qquad \psi_2 = \phi_{Na(3s)}\,, \tag{30}$$

transforming into bonding and antibonding molecular orbitals

$$\psi_1 \approx \phi_{Li(2s)} + \phi_{Na(3s)}\,, \qquad \psi_2 \approx \phi_{Li(2s)} - \phi_{Na(3s)}\,, \tag{31}$$

at small $R(<6a_0)$. [Equation (31) is schematic, since components of ψ_1 and ψ_2 on each nucleus are polarized (p character) and more contracted than for the atoms.] The resulting M_{12} for $LiNa^+$ is shown

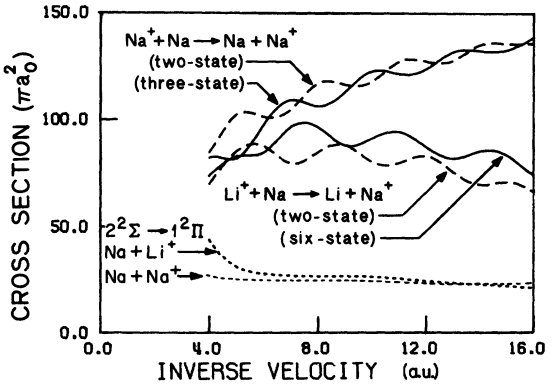

FIG. 9. Total charge-transfer cross sections for $Na + Na^+$ and $Na + Li^+$ in the 3- or 6-state approximation (solid lines) and in the two-state approximation (dashed line). Also plotted are cross sections for transitions of the $2\,^2\Sigma^+$ (or $1\,^2\Sigma_u^+$) state to the $1\,^2\Pi$ (or $1\,^2\Pi_u$) state in the two-state approximation.

in Fig. 7.

For finite velocities one might expect transitions between these adiabatic states throughout the entire coupling region ($R = 6a_0$ to $R = 20a_0$). However, the energy difference between states (shown in Fig. 7) grows exponentially as the atomic orbitals begin to overlap. As a result, the exponential terms in Eq. (8) begin to oscillate rapidly, leading to a zero net transfer between states for smaller R. Thus, transitions between states occur only at large R (between $\sim 12a_0$ and $20a_0$ for $LiNa^+$, the actual width depending on the velocity) where M_{12} is large while ΔE is still small. We denote this region as the *transition region*. For smaller R, the nuclei enter an *intermediate region* in which no net transitions occur between the states. However, since each state represents motion on a different potential energy curve, the phase factors of Eq. (7) will differ, resulting in a phase difference of

$$\Delta\phi = \int_{-R_0}^{R_0} \frac{1}{v}\,\Delta E\,dz, \tag{32}$$

where R_0 is a representative internuclear distance of the transition region. As the nuclei separate, they again pass through the transition region, leading to a decoupling of the molecular states back into atomic states. The different regions are depicted in Fig. 10. If there were no change in phase ($\Delta\phi = 0$), then since $\Gamma(-z) = -\Gamma(z)$, the transition process on the outgoing leg would exactly reverse the transition process on the incoming leg, yielding the original starting state and hence no charge transfer. However, in general, $\Delta\phi$ is not zero, leading to a charge transfer probability that depends on the relative phase change (32) between the two intermediate states.

We thus find that in the molecular-wave-function framework the description of the near-resonant charge-transfer process is comparable to that of the symmetric resonant charge-transfer process (where $R_0 = \infty$).[43] Initially the electron starts out localized on one atom. As the nuclei approach, they pass through a transition region in which the atomic states are coupled into molecular states. Inside the transition region, the electron has a fixed probability $|\bar{a}_i(R_I)|^2$ of being in either of the two molecular states ($|\bar{a}_1|^2 + |\bar{a}_2|^2 = 1$). [For the symmetric case, $|\bar{a}_1(R_I)|^2 = |\bar{a}_2(R_I)|^2 = \frac{1}{2}$.] The magnitudes $|\bar{a}_1|$ and $|\bar{a}_2|$ remain constant in the intermediate region but the phase factors change, leading to a relative phase change of $\Delta\phi$ given by Eq. (32). The nuclei upon separating re-enter the transition region where the molecular states are decoupled back into atomic states. Phase interference yields a transition probability of the form

$$P(v,b) \approx 4|\bar{a}_1\bar{a}_2|^2 \sin^2[\tfrac{1}{2}\Delta\phi], \tag{33}$$

where $\Delta\phi$ is defined in (32).

In the resonant case $|\bar{a}_1| = |\bar{a}_2|$ so that Eq. (33) reduces to Eq. (28). Since $|\bar{a}_1|^2 + |\bar{a}_2|^2 = 1$ we will denote $|a_2|^2$ as p (which depends upon v and b) and rewrite (33) as

$$P(v,b) = 4p(1-p)\sin^2[\tfrac{1}{2}\Delta\phi]. \tag{33'}$$

While P represents the transition probability for the entire process, p represents the transition probability upon crossing the transition region only *once*. As in the symmetric case, P is maximum when the phases of the states interfere ($\Delta\phi = \pi$), and is zero when there is no phase interference ($\Delta\phi = 0$).

The actual transition probabilities for $LiNa^+$ [as obtained from Eq. (8) in the two-state approximation] are shown in Fig. 8(b). In particular, in Fig. 11(a) we have superimposed the transition probabilities P, for $v^{-1} = 6$, 12, and 18 a.u., showing that $P(v,b)$ does indeed have the form $\sin^2[\frac{1}{2}\Delta\phi]$ with $\Delta\phi$ proportional to v^{-1}. The values of $p(v,b)$ for $v^{-1} = 6$, 12, and 18 a.u. are shown in Fig. 11(b). [The p's were obtained by integrating Eq. (8) from $z = -\infty$ to $z = 0$.] Note that no oscillations occur in p since the transition region has only been crossed once.

The processes involved in Π-Π coupling are equivalent to those of the Σ-Σ coupling process [with Eq. (33) representing the transition probability] and will not be discussed here.

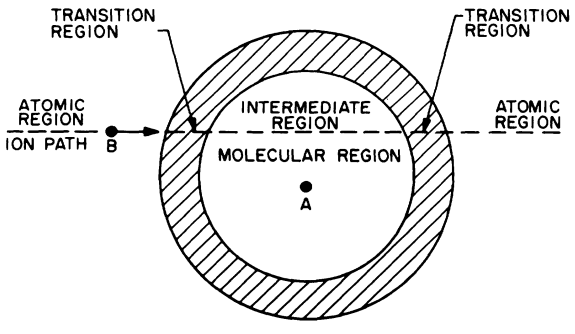

FIG. 10. Diagram illustrating the transition region and the intermediate region of the charge-transfer process.

C. Two-state atomic model for Σ-Σ coupling

In order to better understand the nature of the two-state coupling process, we will consider a simple model in which the molecular wave functions are expressed in terms of an atomic state on each atom. With this model, we will obtain an approximate functional dependence of both p and $\Delta\phi$ upon the velocity and impact parameter.

We will assume here that the molecular wave

functions can be expressed as a linear combination of the two atomic orbitals (at least in the transition region). (These orbitals need not be the actual atomic orbitals but could in fact include hybridization and contraction effects.) Ignoring the overlap between the atomic orbitals in this region (this approximation can be removed, at the cost of an increase in complexity), the molecular wave functions are given by

$$\psi_1(z)=\phi_A\cos[\theta(z)]+\phi_B\sin[\theta(z)],$$
$$\psi_2(z)=-\phi_A\sin[\theta(z)]+\phi_B\cos[\theta(z)], \tag{34}$$

where ϕ_A and ϕ_B are the atomic orbitals. Letting ϵ_A and ϵ_B be the energies of ϕ_A and ϕ_B, respectively, and letting H_{AB} be the interaction Hamiltonian, we have

$$\Delta E=2H_{AB}(\alpha^2+1)^{1/2}, \tag{35}$$

$$\tan\theta=\alpha\pm(\alpha^2+1)^{1/2}, \tag{36}$$

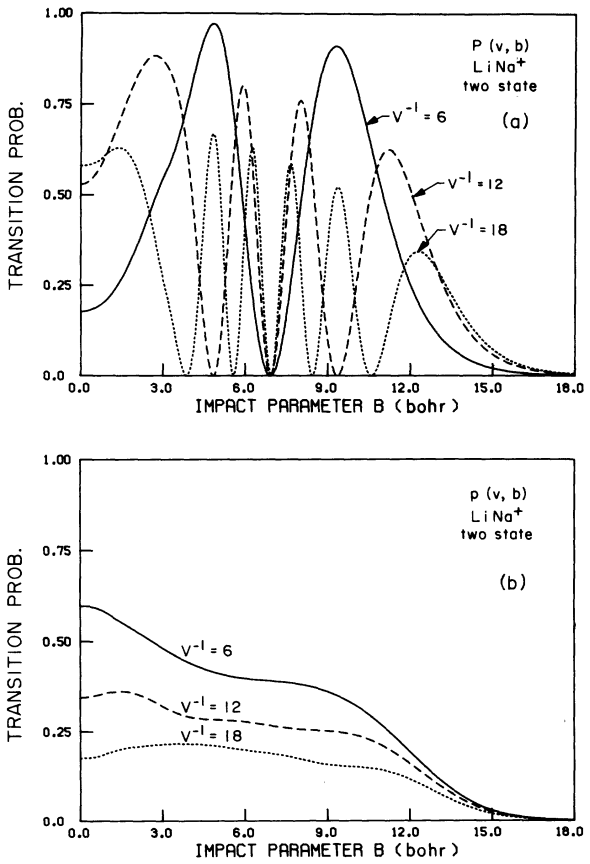

FIG. 11. (a) Transition probabilities $P(v,b)$ for the two-state $Li+Na^+ \rightarrow Li^+ + Na$ charge-transfer process for inverse velocities $v^{-1}=6$, 12, and 18 a.u. (b) Transition probabilities p at $z=0$ for the two-state $Li+Na^+ \rightarrow Li^+ + Na$ charge-transfer process for $v^{-1}=6$, 12, and 18 a.u.

where

$$\alpha=\Delta V_\infty/2H_{AB} \quad \text{and} \quad \Delta V_\infty=|\epsilon_B-\epsilon_A|. \tag{37}$$

Using Eq. (34) the coupling term for $b=0$ is just

$$M_{12}=\langle\psi_1|\frac{\partial}{\partial R}|\psi_2\rangle=\frac{\partial\theta}{\partial R}. \tag{38}$$

That is, the Born-Oppenheimer coupling term for the molecular wave function represents the rate of rotation of the two atomic wave functions between themselves to form the molecular wave functions. The final molecular wave function ($R=0$) corresponds to a rotation of $\frac{1}{4}\pi$.

To obtain an estimate of M_{12} we will take H_{AB} to be decreasing exponentially in the transition region,

$$H_{AB}=\kappa e^{-\beta R}. \tag{39}$$

(This is reasonable, since the terms responsible for bonding change exponentially with R for large R.) The resulting two-state atomic model using H_{AB} given by (39) has been described in earlier papers—for instance, by Rapp and Francis[6] and by Demkov.[8] We define R_M as the midway point in the rotation [i.e., $\theta(R_M)-\theta(\infty)=\frac{1}{8}\pi$], which occurs when $2H_{AB}=\Delta V_\infty$ or $\alpha=1$. Using Eq. (38) and (39) leads to

$$M_{12}=\tfrac{1}{4}\beta\,\mathrm{sech}[\beta(R-R_M)]. \tag{40}$$

For $LiNa^+$, we find from Fig. 7 that M_{12} does indeed have the general form of Eq. (40) in the transition region [fitting (40) to the M_{12} of Fig. 7 leads to $R_M\approx 12.8a_0$ and $\beta\approx 0.42$[44]; this corresponds to $\kappa=1.01$ in Eq. (39)]. [Note that in (40) the value of M_{12} at the maximum ($\frac{1}{4}\beta$) is related to the exponential decay rate β, since the total area under curve for M_{12} must equal the total $\Delta\theta=\theta(0)-\theta(\infty)\approx\frac{1}{4}\pi$.[45]]

Substituting Eq. (40) and Eq. (35) into Eq. (8) and integrating from $z=-\infty$ to $z=0$, leads to the $p(v,b)$ shown in Fig. 12 (solid lines). These approximate results can be compared with the actual p's in Fig. 11(b).

Analytic forms for $p(v,b)$ can be obtained in two limiting cases. For zero impact parameter ($b=0$), $\Gamma_{12}=\pm M_{12}$, since $z=\pm R$. The solution of Eq. (8) then yields

$$p(v,0)=\tfrac{1}{2}\,\mathrm{sech}(\gamma)e^{-\gamma}, \tag{41}$$

where

$$\gamma=\pi\Delta V_\infty/2\beta v. \tag{42}$$

At high velocities ($\Delta V_\infty/v \ll 1$) $p(v,0)=\frac{1}{2}$ (which is equivalent to the symmetric case, for which $\Delta V_\infty/v\equiv 0$). As the velocity goes to zero, $p(v,0)$ goes to zero exponentially as v^{-1}.

The other case that is easy to solve analytically is the high-energy limit. In this case the exponen-

tial terms in Eq. (8) can be ignored, and we obtain

$$p(\infty, b) = \sin^2\{\tfrac{1}{4}\arctan[\sinh(\beta(R_M - b))] + \tfrac{1}{8}\pi\}. \tag{43}$$

Thus $p(\infty, b)$ has a value of $\frac{1}{2}$ at $b = 0$ and eventually dies exponentially to zero at large b. This decrease in p with increasing impact parameter results from the z/R dependence of Γ_{12} [i.e., $\Gamma_{12} = (z/R)M_{12}$]. Thus, for large b, $z = (R^2 - b^2)^{1/2} \ll R$ in the transition region (see Fig. 10).

To obtain an approximate analytical form for $p(v, b)$, we will take p to be a product of $p(v, 0)$ and $p(\infty, b)$, i.e.,

$$p(v, b) \approx 2p(v, 0)p(\infty, b), \tag{44}$$

where $p(v, 0)$ is defined in Eq. (41) and $p(\infty, b)$ is defined in Eq. (43). This approximate p is shown in Fig. 12 (dashed line) and compared with the p obtained from substituting the two-state atomic model into Eq. (8). To complete the atomic eigenfunction model of Eq. (33′), we will obtain an estimate of the phase difference $\Delta\phi$. Ignoring the ΔV_∞ compared to H_{AB} and letting R_0 go to infinity, yields

$$\Delta\phi = (4kb/v)K_1(b\beta), \tag{45}$$

where K_1 is a Bessel function of the second kind. Since K_1 rapidly approaches infinity as $b \to 0$, $\sin^2(\frac{1}{2}\Delta\phi)$ oscillates very rapidly at small b and can be approximated by its average value of $\frac{1}{2}$. However, since K_1 does not possess a maximum, no oscillations are present in the total cross section.

The exponential decrease of the cross-section results from the velocity dependence of p in Eq. (41). The high-energy limit is proportional to v^{-2} due to the v^{-1} dependence of $\Delta\phi$.[46] From Eq. (8) we would expect the maximum in the cross section to occur when both the cosine and sine parts of the exponential term can maintain the same sign throughout the transition region, i.e., when

$$\Delta V_\infty \Delta z / v_{\max} \approx \tfrac{1}{4}\pi, \tag{46}$$

where Δz is a measure of the width of the transition region. [Note that the translational energy of the ion needed to cause an appreciable transition probability is far greater than the energy difference between electronic states (10^3 eV compared to 1 eV).] For $LiNa^+$, $\Delta V_\infty = 0.0093$ a.u. and $v_{\max} \approx 0.14$ a.u., and hence (46) leads to $\Delta z \approx 12a_0$. Eq. (46) is related to the "near-adiabatic" theory proposed by Massey.[47] From Eq. (40), we see that Δz is inversely proportional to β. This property is reflected in the transition probability p [Eq. (41)] which is a function of $\Delta V_\infty/\beta v$.

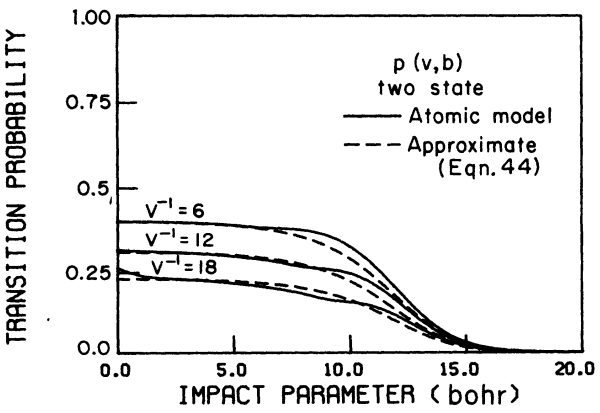

FIG. 12. Transition probabilities p at $z = 0$ for the two-state $Li + Na^+ \to Li^+ + Na$ charge-transfer process using the two-state atomic model (solid) and an approximation [Eq. (44)] (dashed) for $v^{-1} = 6$, 12, and 18 ($\beta = 0.42$, $\Delta V_\infty = 0.0093$ Hartree, and $R_M = 12.8a_0$).

D. Two-state Σ-Π coupling process

The coupling between Σ and Π states results from the rotation of the nuclear axis with respect to the space-fixed axis. The Σ-Π coupling process has been studied in detail in a recent paper by Russek.[15] Russek's model assumes a constant coupling term and intersecting straight line potential energy curves. From Fig. 3 and Fig. 4(b), we see that these approximations are quite good for the $LiNa^+$ $2\,^2\Sigma^+ \to 1\,^2\Pi$ transition [for $LiNa^+$, $\langle 2\,^2\Sigma^+|\partial/\partial\theta|1\,^2\Pi\rangle \approx 0.95$, $R_c \approx 5.1a_0$]. The actual two-state transition probabilities between the $2\,^2\Sigma^+$ and $1\,^2\Pi$ states of $LiNa^+$ are shown in Fig. 8(c) for various velocities.

While $\Gamma_{\Sigma-\Sigma}$ has the general form

$$\Gamma_{\Sigma-\Sigma} \approx (z/R)\tfrac{1}{4}\beta\,\mathrm{sech}[\beta(R - R_M)], \tag{47}$$

[see Eq. (40)], $\Gamma_{\Sigma-\Pi}$ has the form (in the coupling region)

$$\Gamma_{\Sigma-\Pi} \approx (b/R^2)L, \tag{48}$$

where L is a constant. Thus, $\Gamma_{\Sigma-\Pi}$ does not go to zero for small R, but rather, increases. This growth in Γ as R becomes smaller compensates for the corresponding increase in the energy difference, leading to a continuous coupling between the states. Therefore, the phase interference between states is an integral part of the Σ-Π coupling process and oscillations occur throughout the transition (see Ref. 15). While $\Gamma_{\Sigma-\Sigma}$ is zero at the half-way point in the collision (i.e., $z = 0$), $\Gamma_{\Sigma-\Pi}$ reaches its maximum value at this point. Furthermore, $\Gamma_{\Sigma-\Pi}$ maintains the same sign throughout the collision. Thus, unlike Σ-Σ coupling, large transition probabilities occur for collision trajectories tangential to and even outside the curve

crossing [see Fig. 8(c)]. Due to the curve crossing, $P_{\Sigma-\Pi}$ can be large even for small velocities, unlike $P_{\Sigma-\Sigma}$, which decreases exponentially as v^{-1} (see Fig. 10).

Although the curve crossing is at $5.1a_0$ we see in Fig. 8(c) that a significant transition probability $P_{\Sigma-\Pi}$ exists for collision trajectories outside the curve crossing point (i.e., $b>R_c$). The maximum in $P_{\Sigma-\Pi}$ occurs at an impact parameter just inside the curve crossing. For smaller b, $P_{\Sigma-\Pi}$ decreases, eventually becoming zero at $b=0$.[48] Oscillations appear in $P_{\Sigma-\Pi}$ for small b as the velocity decreases. However, the maximum in $P_{\Sigma-\Pi}$ remains close to unity, decreasing very slowly at smaller velocities. Therefore, the total cross section $\sigma_{\Sigma-\Pi}$ for Σ-Π coupling (see Fig. 9) decreases very slowly as v goes to zero (resulting essentially from the narrowing of $P_{\Sigma-\Pi}$ about its maximum). (The cross section for very low velocities can also be estimated from Fig. 7 of Russek's paper.) Since small impact parameters b do not contribute significantly to the total cross section (because $P_{\Sigma-\Pi}$ is small and is weighted by b), no significant oscillations occur in the total cross section due to the oscillation in $P_{\Sigma-\Pi}$ [see Fig. 8(c)].

The resulting Σ-Π transition probability differs from the Σ-Σ transition probability due to the different nature of the Σ-Σ and the Σ-Π coupling processes. The Σ-Σ coupling process could be divided into three parts involving two transition regions and an intermediate region. On the other hand, the Σ-Π coupling process in the molecular-wave-function approach is more appropriately treated as one continuous process. The difference results from the different nature of the coupling terms.

The Σ-Π total cross section also differs from the Σ-Σ total cross section in the high-energy limit. While $\sigma_{\Sigma-\Sigma}$ approaches zero as v^{-2}, $\sigma_{\Sigma-\Pi}$ continues to increase with increasing velocity. However, the cross section should actually decrease to zero as $v\to\infty$. This calculated increase in $\sigma_{\Sigma-\Pi}$ with increasing velocity for very large V is not physical, but rather is a defect of the molecular-wave-function approach, resulting from the neglect of the translational momentum of the electron. While this neglect of the electron's momentum causes an incorrect velocity dependence for $\sigma_{\Sigma-\Sigma}$ as well as $\sigma_{\Sigma-\Pi}$, the error is more serious for Σ-Π coupling than for Σ-Σ coupling owing to the different nature of the coupling processes. For Σ-Σ transitions, the coupling term $\Gamma_{\Sigma-\Sigma}$ is antisymmetric with respect to z $[\Gamma_{\Sigma-\Sigma}(-z)=-\Gamma_{\Sigma-\Sigma}(z)]$. Hence, at high velocities where the phase change $\Delta\phi$ is small, the transition process for $z<0$ is canceled by the transition process for $z>0$. This leads to a zero net charge transfer. On the other hand, for Σ-Π transitions, the coupling term $\Gamma_{\Sigma-\Pi}$ is symmetric with respect to z $[\Gamma_{\Sigma-\Pi}(-z)=+\Gamma_{\Sigma-\Pi}(z)]$. Hence, at high velocities, the transition process for $z<0$ and for $z>0$ are additive rather than cancelling. Thus, Σ-Π total cross sections remain large as $v\to\infty$.[49] (The neglect of the rotational momentum of the electron appears to cause the Σ-Π transition probability to be overestimated at lower energies as well.)

E. Multistate coupling process

Having considered the various types of two-state processes, we now consider the entire coupling process involved in the scattering processes (1) and (2). We find that the multistate coupling process can be interpreted as a series of two-state coupling processes.[50]

In subsection B, we showed that transitions between two Σ states occur only at long range where the potential energy curves are close together; for smaller R, the two Σ states are uncoupled. On the other hand, Σ-Π transitions occur in the region of the curve crossing between the Σ and Π states. From the potential energy curves for the $LiNa^+$ quasimolecule (Fig. 3), we see that the $1\,^2\Sigma^+$ and $2\,^2\Sigma^+$ potential energy curves are nearly degenerate at large $R(R\gtrsim 12a_0)$, permitting a strong Σ-Σ coupling between these states. The other $^2\Sigma^+$ states are much higher in energy, so that no direct transitions will occur to these higher-lying Σ states [except at high energies ($v>0.2$ a.u. $=4\times10^7$ cm/sec)]. On the other hand, the $1\,^2\Pi$ crosses the $2\,^2\Sigma^+$ state at $5.1a_0$, permitting transitions to occur between the $2\,^2\Sigma^+$ and $1\,^2\Pi$ states at small R. There is a curve crossing of the $1\,^2\Pi$ curve and $3\,^2\Sigma^+$ curve at $10.7a_0$, allowing a two-state coupling between these two states. Finally, the $3\,^2\Sigma^+$ and $4\,^2\Sigma^+$ states and the $1\,^2\Pi$ and $2\,^2\Pi$ states have a near resonance at large R, permitting Σ-Σ and Π-Π coupling to occur, respectively, between these two pairs of states. Coupling will not occur between other pairs of states because the energy difference is too large. Since Σ-Σ transitions (or Π-Π transitions) occur at large R, while Σ-Π transitions occur at small R for which the Σ states are uncoupled, we can decompose the multistate process into separate two-state processes.

First, as the nuclei approach each, the electron entering on the $1\,^2\Sigma^+$ or the $2\,^2\Sigma^+$ state passes through the transition region coupling the $1\,^2\Sigma^+$ and $2\,^2\Sigma^+$ states. The probability for a transition is given approximately by Eq. (44). For smaller R an electron in the $1\,^2\Sigma^+$ state is not coupled with any other state until the nuclei separate and re-

enter the $1\,^2\Sigma^+$-$2\,^2\Sigma^+$ transition region. On the other hand, an electron in the $2\,^2\Sigma^+$ state is coupled to the $1\,^2\Pi$ state at smaller R. This transition between the $2\,^2\Sigma^+$ and $1\,^2\Pi$ states can be considered in terms of the two-state process considered in Sec. IV D. Thus, as the nuclei begin to separate, there is a nonzero probability for being in the $1\,^2\Sigma^+$, $2\,^2\Sigma^+$, and $1\,^2\Pi$ states. As the nuclei separate further, a transition can occur between the $1\,^2\Pi$ state and the $3\,^2\Sigma^+$ state (at $\sim 10.7a_0$). Finally, for $R > 12a_0$, the separating nuclei enter the transition regions for the $1\,^2\Sigma^+$-$2\,^2\Sigma^+$ coupling, $1\,^2\Pi$-$2\,^2\Pi$ coupling, and $3\,^2\Sigma^+$-$4\,^2\Sigma^+$ coupling. For the $1\,^2\Sigma^+$-$2\,^2\Sigma^+$ coupling, the resulting transition probability is no longer given by Eq. (33), but the same basic principles still hold. The probability amplitude on the $2\,^2\Sigma^+$ state in the intermediate region has been reduced because of transitions to the $1\,^2\Pi$ state. Thus, when the atoms depart there is a smaller component of the $2\,^2\Sigma^+$ state to interfere with the $1\,^2\Sigma^+$ state, giving rise to a smaller average P than would be expected from (33). Also, $\Delta\phi$ has been changed due to the new possible trajectories allowed by the presence of the $1\,^2\Pi$ state. If p' represents the probability to remain on the $2\,^2\Sigma^+$ state after the intermediate step, then Eq. (33′) becomes

$$P = 4p(1-p)[p' \sin^2(\tfrac{1}{2}\Delta\phi') + \tfrac{1}{4}(1-p')]. \tag{49}$$

This can be best shown for the symmetric Na_2^+ charge transfer, whose transition probabilities for the three-state process ($1\,^2\Sigma_g^+$, $1\,^2\Sigma_u^+$, $1\,^2\Pi_u$) are shown in Fig. 8(d) [in this case, $p = \frac{1}{2}$ in Eq. (49)]. Since the $\Delta\phi$ changes for the three-state case, the oscillations in the total cross section for Na_2^+ change (see Fig. 9). The corresponding transition probabilities for $Na + Li^+$ in the three-state approximation are shown in Fig. 8(e). Again, the change in $\Delta\phi$ leads to a shift in the oscillations in the $1\,^2\Sigma^+ \rightarrow 2\,^2\Sigma^+$ cross sections (see Figs. 6 and 9). Note that the $2\,^2\Sigma^+ \rightarrow 1\,^2\Pi$ transition probabilities are similar for the two- and three-state approximations except for a scaling factor $(1-p)$, where p is defined in Eq. (33′). [For Na_2^+, $(1-p) \equiv \frac{1}{2}$, so that the two-state Σ-Π transition probability (not shown) is equivalent to the Σ-Π transition probability in the three-state approximation, but scaled by a factor of 2].

In the three-state approximation, the $1\,^2\Pi$ state is not allowed to interact with the other higher lying states. From the potential energy curves, though, we would expect transitions to occur from the $1\,^2\Pi$ state to the $3\,^2\Sigma^+$ and $2\,^2\Pi$ states and then from the $3\,^2\Sigma^+$ state to the $4\,^2\Sigma^+$ state. Since small impact parameters are required to populate the $1\,^2\Pi$ state, however, we would expect the $1\,^2\Pi \rightarrow 3\,^2\Sigma^+$ transition probability will be small. Also, since the Li($2p$)-Na($3p$) energy splitting (0.0187 Hartree = 0.51 eV) is larger than the Li($2s$)-Na($3s$) energy splitting, we would expect the $3\,^2\Sigma^+ \rightarrow 4\,^2\Sigma^+$ and $1\,^2\Pi \rightarrow 2\,^2\Pi$ transition probabilities to be small. From the cross sections shown in Fig. 6, we see that this is indeed the case. The resulting transitions to excited states do not involve interference effects (as in 1Σ-2Σ coupling) since the transition region is only crossed once.

F. Comparison of the molecular-wave-function and the atomic-eigenfunction formulations

We have used the molecular-wave-function formulation (MWF) to obtain charge-transfer cross sections. In this approach, the $\underline{S}$ and $\underline{V}$ matrices of Eq. (4) are diagonal so that the coupling between (molecular) states results purely from the $\underline{\dot{\Gamma}}$ matrix [Eq. (11)]. On the other hand, one could have used the diabatic representation involving (frozen) atomic orbitals in Eq. (4) and would have obtained an equivalent solution (assuming an infinite number of states). In this atomic-eigenfunction formulation (AEF), $\underline{\dot{\Gamma}}$ is assumed to be zero (neglecting the overlap between atomic states), with the coupling between (atomic) states resulting from the nonzero matrix $\underline{V}$. Using the impact-parameter method, the resulting two-state coupled equations in the diabatic representation are[6]

$$\frac{d}{dz}(a_1) = \left(\frac{-i}{v}\right)\frac{H_{AB} - SH_{BB}}{1-S^2} e^{-i\Omega(z)} a_2$$

and (50)

$$\frac{d}{dz}(a_2) = \left(\frac{-i}{v}\right)\frac{H_{AB} - SH_{AA}}{1-S^2} e^{+i\Omega(z)} a_1,$$

where

$$\Omega(z) = \frac{1}{v}\int_{-\infty}^{z} [(H_{BB} - H_{AA})/(1-S^2)]\,dz,$$

$$S = \langle \phi_A | \phi_B \rangle,$$

$$H_{AB} = \langle \phi_A | \mathcal{H}_{el} | \phi_B \rangle.$$

Usually, one further assumes that $S \approx 0$ and that $H_{BB} - H_{AA} \approx \epsilon_B - \epsilon_A$ (for systems like $A + B^+ \rightarrow A^+ + B$).

The resulting equations look very similar to Eq. (8), but differ in two important respects. First, since $\epsilon_B - \epsilon_A$ is a constant, the exponential terms in Eq. (50) oscillate uniformly (assuming $S = 0$) along the entire trajectory. Second, the coupling term H_{AB}/v increases rapidly as the internuclear distance decreases and depends inversely upon the velocity. Thus, in the AEF, we have transitions throughout the entire interaction region, with the strongest coupling at small R. This gives rise to strong oscillations in the transition probability

during the entire collision.

If one were to make the approximations presented in Sec. IV C (i.e., taking the two-molecular states to be linear combinations of the two atomic orbitals with zero overlap and straight line trajectories), then the resulting transition probabilities for the MWF would be identical for either formulation. For example, substituting Eq. (41) into Eq. (33′), we obtain the same transition probability for zero impact as Demkov[8] [Eq. (11) of his paper] obtained using the AEF.[51]

However, as the nuclei are brought together, the molecular wave function ψ_i exhibits a contraction about each nucleus and a polarization toward the other nucleus. These changes are an essential part of the bond formation process. To describe such changes with the AEF requires many atomic eigenfunctions, including the continuum. To see what effect the two-state atomic eigenfunction formulation has on the cross section, we carried out a calculation using the Li(2s) and Na(3s) frozen orbital orbitals as the basis set. The resulting $\Delta E'$ and M'_{12} are compared with the actual ΔE and M_{12} in Fig. 13. We see that for larger R, $\Delta E'$ is smaller than ΔE, and that $\Delta E'$ does not properly describe the maximum responsible for the oscillations in the total cross sections. In addition, M'_{12} is shifted inward with respect to M_{12} and is smaller than M_{12}. This error results primarily from a lack of polarization of the orbitals, which would have allowed interaction of the states at larger R. As a result, the AEF leads to cross sections that are too small.

We saw in Sec. IV C that the actual ΔE and M_{12} could be described by a simple two-state atomic model, with $\beta = 0.42a_0^{-1}$ and $R_M = 12.8a_0$ in Eq. (40). Since this model was based upon the AEF,

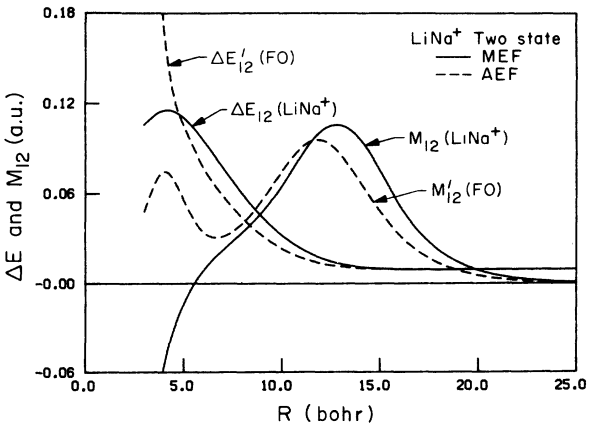

FIG. 13. Comparison of the coupling terms M and M' and the energy difference ΔE and $\Delta E'$ for the complete basis-set calculation and for the frozen orbital (FO) calculation of $LiNa^+$.

one would expect that $\Delta E'$ and M'_{12} would also be described well by the model. However, such is *not* the case. We see from Fig. 13 that M'_{12} is not described well by Eq. (40). The atomic model assumes that the area under the curve M_{12} equals $\frac{1}{4}\pi$. Thus, as M_{12} becomes more localized about R_M, the value of M_{12} at R_M should become larger. The opposite, however, is true of M'_{12}. While M'_{12} is more localized than M_{12}, the maximum value of M'_{12} is less than that of M_{12}. The decay rate of M_{12} about $R'_M = 11.8a_0$ corresponds to $\beta' = 0.46a_0^{-1}$, while the maximum of M'_{12} at R'_M would imply that $\beta' = 0.38a_0^{-1}$.

One can make an additional approximation in the atomic eigenfunction approach by using an empirical formula to obtain β.[6,8,11] One usually takes $\beta = (2I)^{1/2}$ (defined in Hartree atomic units) where I is the smaller of the ionization energies for atoms A and B (although Olson[11] modifies his β by an empirical factor).[52] For $LiNa^+$, this empirically determined value of $\beta\,[=(2I)^{1/2}]$ is $0.62a_0^{-1}$ compared with the value of $0.42a_0^{-1}$ obtained by fitting the calculated M_{12}. Such an overestimation of β (with a corresponding R_M that is too small) leads to a cross section that is too small (see, for example, Ref. 11).

One must be careful to note that the poor results obtained using the β and R_M obtained from the atomic wave functions does not imply that the atomic model presented in Sec. IV C is poor. For $\beta = 0.42$ and $R_M = 12.8a_0$ (obtained by fitting to the MWF results), we in fact obtain a very good approximation of the cross section using this simple atomic model. Thus, the main drawback to the AEF approach is that the β and R_M cannot be estimated by considering atomic quantities. With the appropriate β and R_M, obtained perhaps from a simple MO calculation, one might expect good results. [With good values for β and R_M the reduced cross section presented in Olson's paper[11] should be quite useful for estimating the charge transfer cross sections.]

In addition to the above mentioned drawbacks of the usual two-state AEF for describing the charge transfer process at low energies, the simple picture of multistate charge transfer process presented in Sec. IV E is lost. We found in the MWF that the total transition process could be expressed in terms of a succession of two-state processes. To obtain an estimate of the transition probability to other states in the MWF, we need only know p, the probability for being in an intermediate molecular state [Eq. (44)]. On the other hand, for the AEF the transition region extends throughout the entire interaction region, so that no such noninteracting intermediates exist.

While the AEF provides only the total transition

probability P, one can partition this P into the form given by Eq. (33′), and estimates of this form of P have been made by Rapp and Francis[6] and by Demkov.[8] Using Eq. (51) of Ref. 6, we obtain

$$p_{RF} = \tfrac{1}{2}\,\mathrm{sech}(\gamma_{RF})e^{-\gamma_{RF}},$$
$$\gamma_{RF} = (\pi\Delta V_\infty/2\beta v)(2\beta b/\pi)^{1/2}, \tag{51}$$

while from Eq. (11) of Ref. 8, we obtain

$$p_D = \tfrac{1}{2}\,\mathrm{sech}(\gamma_D)e^{-\gamma_D},$$

with (52)

$$\gamma_D = (\pi\Delta V_\infty/2\beta v)(1 - b^2/R_M^2)^{-1/2},$$

where R_M and β have the same meaning as in Eq. (40). These estimates of p can be compared with our estimate of p (denoted $p_{MG,A}$) obtained in the atomic model with approximation [Eq. (44)] as well as with the p obtained from the numerical evaluation of the two-state atomic model ($P_{MG,N}$). In Fig. 14 we show the p's obtained for $v = 12$, $\beta = 0.42$, $R_M = 12.8a_0$, and $\Delta V_\infty = 0.0093$ Hartree. We see that $P_{MG,N}$, p_D, and $p_{MG,A}$ agree for small b. However, p_D goes to zero at R_M. On the other hand, p_{RF} is an asymptotic approximation for large b, and is not expected to be good at small b. However, even for large b, p_{RF} decreases too slowly.

Another difference between the MWF and the AEF approaches occurs when the rectilinear trajectory restriction is lifted. So far we have considered large incident ion energies ($E > 100$ eV) for which the nuclear trajectory is nearly a straight line, independent of the various potential energy curves upon which the nuclei can move. However, as the incident energy is decreased, the nuclear motion will no longer be linear. It is therefore useful to know the potential energy curve "seen" by the nuclei in order to understand the trajectory of the nuclei during and after the collision.

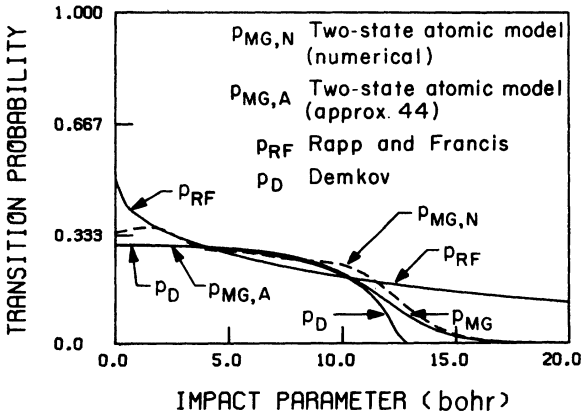

FIG. 14. Comparison of the transition probabilities p using Eq. (44) ($p_{MG,A}$), Eq. (51) (p_{RF}), and Eq. (52) (p_D) and the actual numerical integration of the two-state atomic model ($p_{MG,N}$) for $v^{-1} = 12$ a.u. (see Fig. 12).

The MWF approach presents a simple picture. In the region where the transitions occur, we found that the translational energy must be much greater than the potential energy difference. In this transition region, therefore, we can treat the trajectories for either state as being essentially identical, since the change in potential energy is negligible compared to the nuclear kinetic energy (this is also pointed out in a paper by Delos, Thorson, and Knudson[53]). When the energy difference is large, however, there is no net coupling between states and the nuclei move on one or the other of the adiabatic curves. One can interpret each molecular state as having an electron jumping back and forth between the two atoms. Thus the oscillations in the transition probability [Eq. (33)] can be interpreted as the difference in the electron jumping rates for the two different molecular states. This is much like the mechanism in an interferometer.

On the other hand, no such simple picture is obtained in the diabatic AEF representation. Transitions occur constantly between the diabatic states inside the interaction region. Indeed, these "transitions between atomic states" indicate that the electron does not want to be in a diabatic atomic state at small internuclear distances, but rather it wants to be in an adiabatic molecular state.

We therefore, disagree with the conclusions reached by Penner and Wallace[54] and by Corrigall, Kuppers, and Wallace.[55] While we interpret the transfer process as involving two different trajectories with a given probability for being on each state [$|\bar{a}_1|^2$ and $|\bar{a}_2|^2$ of Eq. (33)], Wallace *et al.*, attempt to define a single trajectory for the entire process. Their conclusion results from a misinterpretation of the meaning of a molecular wave function as well as from a misinterpretation of the transition probability as a function of the trajectory. Our conclusion from the results presented in this paper indicate that semiclassical trajectories defined by adiabatic potential energy curves from molecular wave functions can correctly describe most collisional processes.[56]

The reason that the molecular-wave-function approach is so appropriate is that for collisional energies for which the electron is moving much faster than the nuclei, the electron has time to adjust its motion in order to define a particular energy state (within energy limits resulting from the uncertainty principle). Generally, the energy splitting between the states will be larger than the energy uncertainty. Therefore, the states will be essentially uncoupled. Only for pseudo-curve-crossing regions and for near degeneracies will

the energy uncertainty be of the same size as the energy splitting to allow transitions.

V. CONCLUSION

The multistate molecular-wave-function approach has been used to obtain accurate total charge transfer cross sections. While this in itself is sufficient to establish the usefulness of the approach, we have also shown that the molecular-wave-function approach provides a conceptually simple picture of the charge transfer process, involving a succession of elementary two-state coupling processes. From an understanding of the potential energy curves and molecular wave functions, one can therefore obtain qualitative estimates of the transitions that will occur in other, more complicated collisions. The molecular-wave-function approach should be valid in general for electronic excitation and de-excitation processes, as well as for charge transfer.

---

†Partially supported by a grant (GP-15423) from the National Science Foundation and by a grant (PF-013) from the President's Fund of the California Institute of Technology.

*Based on Ph.D. thesis submitted to the California Institute of Technology, 1972.

‡Present address: Sandia Laboratories, Albuquerque, New Mexico 87115.

§Contribution No. 4759.

[1]L. Landau, Phys. Z. Sowjetunion 2, 46 (1932).

[2]C. Zener, Proc. Roy. Soc. Lond. A 137, 696 (1932).

[3]E. C. G. Stueckleberg, Helv. Phys. Acta 5, 369 (1932).

[4]For a recent discussion of the LZS Method, see W. R. Thorson, J. B. Delos, and S. A. Boorstein, Phys. Rev. A 4, 1052 (1971).

[5]E. G. Gurnee and J. L. Magee, J. Chem. Phys. 26, 1237 (1956).

[6]D. Rapp and W. E. Francis, J. Chem. Phys. 37, 2631 (1962).

[7]D. R. Bates, Dis. Faraday Soc. 33, 7 (1962).

[8]Y. N. Demkov, Sov. Phys.—JETP 18, 138 (1964).

[9]A. R. Lee and J. B. Hasted, Proc. Phys. Soc. 85, 673 (1965).

[10]W. Lichten, Phys. Rev. 139, A27 (1965).

[11]R. E. Olson, Phys. Rev. A 6, 1822 (1972).

[12]M. Born and J. R. Oppenheimer, Ann. Phys. (Leipz.) 84, 457 (1927).

[13]D. R. Bates and D. A. Williams, Proc. Phys. Soc. 83, 425 (1964).

[14]R. McCarroll and R. D. Piacentini, J. Phys. B 4, 1026 (1971).

[15]A. Russek, Phys. Rev. A 4, 1918 (1971).

[16]R. K. Colegrave and D. B. L. Stephens, J. Phys. B 1, 856 (1968).

[17]S. A. Evans, J. S. Cohen, and N. F. Lane, Phys. Rev. A 4, 2235 (1971).

[18]W. L. McMillan, Phys. Rev. A 4, 69 (1971).

[19]C. Bottcher and M. Oppenheimer, J. Phys. B 5, 492 (1972).

[20]D. W. Jepsen and J. O. Hirschfelder, J. Chem. Phys. 32, 1323 (1960).

[21]See, for example, D. R. Bates and A. R. Holt, Proc. Roy. Soc. Lond. A 292, 168 (1966).

[22]This should be valid except for very small impact parameters, which contribute little to the total cross section.

[23]D. R. Bates, H. S. Massey, and A. L. Stewart, Proc. Roy. Soc. Lond. A 216, 437 (1953).

[24]For details of the numerical techniques used to solve Eq. (8), see C. F. Melius, Ph.D. thesis, California Institute of Technology, 1972. A fixed step size (involving 200 to 300 points) was used, the $a_i(+\infty)$ being accurate to three places. The impact parameter was varied in increments of $0.25a_0$ to $0.5a_0$, while the velocity was incremented by 1.0 a.u. of inverse velocity.

[25](a) I. V. Abarenkov and V. Heine, Philos. Mag. 12, 529 (1965); (b) A. Dalgarno, C. Bottcher, and G. A. Victor, Chem. Phys. Lett. 7, 265 (1970); (c) G. Simons, J. Chem. Phys. 55, 756 (1971).

[26]See (a) C. F. Melius, W. A. Goddard III, and L. R. Kahn, J. Chem. Phys. 56, 3342 (1972); (b) C. F. Melius and W. A. Goddard III, Phys. Rev. A 10, 1528 (1974); (c) L. R. Kahn and W. A. Goddard III, J. Chem. Phys. 56, 2685 (1972); (d) W. A. Goddard III, Phys. Rev. 174, 659 (1968).

[27]D. R. Bates and R. McCarroll, Proc. Roy. Soc. Lond. A 245, 175 (1958).

[28]S. B. Schneiderman and A. Russek, Phys. Rev. 181, 311 (1969).

[29]H. Levy II and W. R. Thorson, Phys. Rev. 181, 252 (1969).

[30]M. E. Riley and T. A. Green, Phys. Rev. A 4, 619 (1971).

[31]R. McCarroll, Proc. Roy. Soc. Lond. A 284, 547 (1961).

[32]T. A. Green, Proc. Phys. Soc. 86, 1017 (1965).

[33]The translational momentum of the electron will be important when the energy difference ΔE between states is zero. For large R, $\Delta E = 0$ in the symmetric resonant case. In this case, neglect of translational momentum prevents the symmetric molecular states from dissociating correctly to left and right atomic states, resulting in a nonzero coupling between states.

[34]C. F. Melius and W. A. Goddard III, Chem. Phys. Lett. 15, 524 (1972).

[35]Other choices of the weighting factor are possible. For instance, one could choose

$$\rho_{ij}(\vec{r}) = |\psi_i(\vec{r})|^2 |\psi_j(\vec{r})|^2.$$

[36]The results for collisions of other alkali-metal systems will be presented in a separate paper [C. F. Melius and W. A. Goddard III, (unpublished)].

[37]H. L. Daley and J. Perel, VIth ICPEAC, MIT, Cambridge (MIT Press, Cambridge, 1969), p. 1051.

[38]J. Perel (private communication).

[39]The neglect of the electron's momentum appears to be

more serious in Σ-Π transitions than in Σ-Σ transitions (Ref. 36). As a result, the total cross section for the endothermic process (Eq. 1) can be too small at low velocity.

[40]O. B. Firsov, Zh. Eksp. Teor. Fiz. 21, 1001 (1951).

[41]F. J. Smith, Phys. Lett. 20, 271 (1966).

[42]J. Perel, Phys. Rev. A 1, 369 (1970).

[43]When electron momentum is included, R_0 for the symmetric case also becomes finite.

[44]For small R, the actual M_{12} differs from Eq. (40) due to the interaction with the core electrons. However, since this is inside the transition region, it does not significantly affect the results.

[45]For the case of near curve crossing, $\Delta\theta \approx \frac{1}{2}\pi$. However, instead of M_{12} being given by Eq. (40), M_{12} is Lorentzian in shape, being strongly peaked at the pseudo crossing point, i.e.,

$$M_{12} = \tfrac{1}{2}(\xi/2H_{12})[1 + (\xi/2H_{12})^2(R - R_c)^2]^{-1},$$

where ξ is the difference in the slopes of the diabatic potential energy curves at the crossing point.

[46]Since the electron's translational momentum has been ignored, the exact $\sigma_{\Sigma-\Sigma}$ should fall off faster than v^{-2}.

[47]H. S. W. Massey, Rept. Progr. Phys. 12, 248 (1949).

[48]The reason that the transition probability is small for small impact parameters is that the wave function tends to remain space-fixed while the nuclei rotate. Since the rotation is almost 180° (for a rectilinear trajectory), the resulting wave function still has the original symmetry (though the phase of the molecular wave function may change).

[49]The Σ-Π cross section eventually becomes flat at high velocity since $\langle 2\,^2\Sigma|\partial/\partial\theta|1\,^2\Pi\rangle$ eventually goes to zero at large R. In the model used by Russek, the coupling term is assumed constant for all R, but the energy difference is assumed to be infinite at large R, so his cross section also becomes flat at high velocity.

[50]C. F. Melius and W. A. Goddard, III, Phys. Rev. Lett. 29, 975 (1972).

[51]For the $\sin^2(\Delta\phi)$ term, Demkov neglects the ΔV_∞ term, while we leave it in but require a finite range of integration. Demkov in his derivation uses the diabatic representation [rather than the adiabatic representation as he implies in Eq. (6)]. Also, as we showed, the transition region occurs over a wide region; this region is generally outside Demkov's R_0(≡ our R_M), since the energy difference is smaller. Instead of Eq. (11) of Demkov's paper (which implies that the transition occurs at a discrete point), one should use Eq. (44) substituted into Eq. (33′) (which was obtained using the molecular-wave-function approach). The basic ideas presented in Demkov's paper are correct, however, as we have shown. Demkov would estimate β of Eq. (39) to be $\beta = (2I)^{1/2}$(=$0.62a_0^{-1}$ for $LiNa^+$), while we find that $\beta = 0.42a_0^{-1}$.) However, this inaccuracy in approximating β results from the approximation of H_{AB} and does not reflect on the interpretation of the results in his paper.

[52]Olson (Ref. 11) has attempted to improve upon the common approximation for β by taking $\beta = 0.86(2I)^{1/2}$, where the factor (0.86) is obtained from experimental observation. He obtains an $R_M = 10.63a_0$. While H_{AB} could have been put in the form (32) with $\kappa = 1.3$ and $\beta = 0.535$ (by taking $R \approx R_M$), Olson takes $\kappa \equiv 1.0$ and obtains a final value $\beta = 0.506$.

[53]J. B. Delos, W. R. Thorson, and S. K. Knudson, Phys. Rev. A 6, 709 (1972).

[54]A. Penner and R. Wallace, Phys. Rev. A 5, 639 (1972).

[55]B. Corrigall, K. Kuppers, and R. Wallace, Phys. Rev. A 4, 977 (1971).

[56]For Σ-Π coupling, we found that the molecular-wave-function approach leads to coupling throughout the entire coupling region. The reason is that the molecular wave functions do not provide the optimal representation. The optimal representation involves angular-momentum states defined by $(\Sigma + i\lambda\Pi)/(1+\lambda^2)^{1/2}$ and $(\lambda\Sigma - i\Pi)/(1+\lambda^2)^{1/2}$, where λ depends on R and v. In this new representation, the coupling process would then involve a transition region (near the pseudo-curve crossing) and an intermediate region. The resulting potential energy curves would provide the appropriate trajectory paths.